Acta Biomaterialia xxx (2015) xxx–xxx

Contents lists available at ScienceDirect

Acta Biomaterialia

journal homepage: www.elsevier.com/locate/actabiomat

# Nanocolumnar coatings with selective behavior towards osteoblast and *Staphylococcus aureus* proliferation

Isabel Izquierdo-Barba [a,b], José Miguel García-Martín [c], Rafael Álvarez [d], Alberto Palmero [d], Jaime Esteban [e], Concepción Pérez-Jorge [e], Daniel Arcos [a,b,*], María Vallet-Regí [a,b,*]

[a] Departamento de Química Inorgánica y Bioinorgánica, Facultad de Farmacia, Universidad Complutense de Madrid, Instituto de Investigación Sanitaria Hospital 12 de Octubre i+12, Plaza Ramón y Cajal s/n, 28040 Madrid, Spain
[b] CIBER de Bioingeniería, Biomateriales y Nanomedicina (CIBER-BBN), Spain
[c] IMM-Instituto de Microelectrónica de Madrid (CNM-CSIC), Isaac Newton 8, PTM, E-28760 Tres Cantos, Madrid, Spain
[d] Instituto de Ciencia de Materiales de Sevilla (CSIC-Universidad de Sevilla), Americo Vespucio 49, 41092 Seville, Spain
[e] Department of Clinical Microbiology, IIS-Fundación Jiménez Díaz, Universidad Autónoma de Madrid, Spain

ARTICLE INFO

*Article history:*
Received 28 October 2014
Received in revised form 16 December 2014
Accepted 23 December 2014
Available online xxxx

*Keywords:*
Titanium nanocolumns
Magnetron sputtering
Biocompatibility
Antibacterial effects
Biofilm

ABSTRACT

Bacterial colonization and biofilm formation on orthopedic implants is one of the worst scenarios in orthopedic surgery, in terms of both patient prognosis and healthcare costs. Tailoring the surfaces of implants at the nanoscale to actively promote bone bonding while avoiding bacterial colonization represents an interesting challenge to achieving better clinical outcomes. Herein, a Ti6Al4V alloy of medical grade has been coated with Ti nanostructures employing the glancing angle deposition technique by magnetron sputtering. The resulting surfaces have a high density of nanocolumnar structures, which exhibit strongly impaired bacterial adhesion that inhibits biofilm formation, while osteoblasts exhibit good cell response with similar behavior to the initial substrates. These results are discussed on the basis of a "lotus leaf effect" induced by the surface nanostructures and the different sizes and biological characteristics of osteoblasts and *Staphylococcus aureus*.



## 1. Introduction

Orthopedic prosthetic implants save and/or improve the quality of life of millions of patients every year [1]. On the basis of their excellent biocompatibility and good mechanical properties, some metallic alloys are generally employed to manufacture devices such as join prostheses, fracture fixation elements and external fixators. One of the most serious complications of prosthetic devices, in terms of morbidity, mortality and medical costs, is the incidence of infection [2]. Even though its occurrence has significantly diminished thanks to clinical staff training, control of sterility and protocols of antibiotic prophylaxis, a marginal risk as low as 0.5–5% (for total join arthroplasty) implies that thousands of prostheses and other orthopedic devices are infected every year [3,4] – an issue of increasing relevance, due to the larger number of patients who undergo prosthetic joint surgery today.

Most of the infections in metallic orthopedic implants are caused by staphylococci [5]. Among them, *Staphylococcus aureus* and *S. epidermidis* are the two most active species on metallic biomaterials, e.g. stainless steel, CrCo, Ti and Ti alloys [6,7]. In this regard, it is well known that, once bacteria attach to the implant surface, a biofilm is formed that provides antibiotic resistance, becoming the main pathogenic factor for chronic infections [8–10]. In fact, one of the milestones in this research field consists in the development of implant surfaces that diminish the bacterial adherence and the formation of the biofilm. Campoccia et al. [11] have reviewed different technologies aimed at developing infection-resistant surfaces, and other reports indicate that the use of nanostructured surfaces with inhibited bacterial adhesion could represent a challenging alternative to antibiotics [12–14]. Several research groups have demonstrated that nanostructured biomaterials may improve the response of osteoblasts [15–17], and Anselme et al. have highlighted [18] that the development of surfaces with simultaneous opposite responses towards osteoblasts and bacterial proliferation would represent a significant achievement in orthopedic implantology. In the literature, there are very few studies that analyze surfaces that fulfill both conditions, and there are none on materials employed in the manufacture of orthopedic

* Corresponding authors at: Departamento de Química Inorgánica y Bioinorgánica, Facultad de Farmacia, Universidad Complutense de Madrid, Instituto de Investigación Sanitaria Hospital 12 de Octubre i+12, Plaza Ramón y Cajal s/n, 28040 Madrid, Spain. Tel.: +34 913941843.
*E-mail addresses:* arcosd@ucm.es (D. Arcos), Vallet@ucm.es (M. Vallet-Regí).

http://dx.doi.org/10.1016/j.actbio.2014.12.023
1742-7061/

devices [19,20] with the exception of Ref. [21], which focuses on commercially pure Ti for dental applications. The idea of tailoring surfaces with customized and selective responses towards specific cell types was also suggested by Decuzzi and Ferrari [22]. They proposed a mathematical model that indicated the key role of the surface nanotopography in the stimulation of osteoblast-like cells while reducing bacterial adhesion and proliferation. In a recent publication, the antibacterial activity of nanostructured titanium surfaces fabricated on silicon wafers has been reported [23], showing that these were active against Gram-negative *Escherichia coli* but inefficient against Gram-positive *S. aureus*. As stated by the authors, these coatings "are not meaningful in the orthopedic field, in which a very large proportion of all implant-related infections are caused by staphylococci". Overall, and regarding the state of the art in the area of orthopedic implants, a significant advance in the development of infection-resistant coating (prior to an in vivo analysis) should comprise the following features: (i) it must be tested on substrates made of medical grade biomaterials; (ii) it should not diminish the adhesion and proliferation of human osteoblasts; (iii) it should exhibit antibacterial behavior against the most pathogenic bacteria in orthopedic-related infections, and in particular it should avoid the formation of the biofilm; and (iv) it should present antibacterial properties with respect not only to collection strains but also to clinical ones, i.e. those isolated from patients with infection, since their behavior can be different.

Herein, we report the preparation of nanocolumnar patterned surfaces made of titanium by means of the so-called glancing angle deposition technique by magnetron sputtering (MS-GLAD). MS-GLAD is a powerful technique for producing nanostructured coatings in large areas and with a large variety of morphologies [24,25]. It is based on exploiting atomic shadowing effects during physical vapor deposition under high vacuum conditions. MS-GLAD is widely employed in microelectronics as well as in other fields of nanotechnology, both in research and in industrial mass-production facilities, due to the high growth rate of the obtained coatings, the possibility of working on large areas at room temperature and its versatility in fine-tuning atomistic self-assembly processes on surfaces [26]. We have recently studied MS-GLAD in detail [24,27], and we have demonstrated that the main processes responsible for the formation of the nanostructures are the atomic self-shadowing mechanism at the surface and the collisional processes of the sputtered atoms in the plasma phase, mediated by the tilt angle of the substrate and the value of the argon background pressure.

Our ultimate aim is to prepare nanocolumnar coatings made of Ti on typical orthopedic device material (Ti6Al4V) that preserve the biocompatibility towards osteoblast while the *S. aureus* adherence dramatically falls. Furthermore, the formation of a biofilm of such bacteria should be inhibited, which is a key factor in preventing the infection of a prosthesis. To our knowledge, this is the first experimental demonstration of a nanostructured coating on medical grade Ti6Al4V exhibiting compatibility towards osteoblast adhesion and proliferation whilst reducing *S. aureus* adhesion, proliferation and biofilm formation.

## 2. Materials and methods

### 2.1. Fabrication of the nanostructured coating

Medical grade Ti6Al4V substrates of 12 mm diameter and 2 mm thickness (Biomet Spain Orthopedic S.L.) were mechanically polished to a mirror finish by a sequence of diamond pastes until colloidal silica (0.25 μm) finishing. Such disks were used as substrates to be coated with titanium nanocolumns by MS-GLAD. For this purpose, a Ti vapor flux was produced by the magnetron sputtering technique employing a 5 cm diameter Ti target, with argon as the sputter gas. The substrates were placed 22 cm away from the target and tilted 80° with respect to its normal. The base pressure of the chamber was in the mid-$10^{-9}$ mbar range, whereas the deposition was carried out at a pressure of $1.5 \times 10^{-3}$ mbar, employing a DC electromagnetic power generator set at 300 W. Under these conditions, the deposition rate was 0.3 Å $s^{-1}$ and the substrate temperature was always below 330 K during the growth of the nanostructured coating. Only one surface of the disks was coated. The coated Ti6Al4V substrates are hereinafter referred to as Nano-Ti6Al4V. For comparison purposes, uncoated substrates of the same medical grade Ti6Al4V were included in all the experiments.

### 2.2. Material surface characterization

Powder X-ray diffraction (XRD) patterns were recorded with a Philips Model X'Pert diffractometer using Cu $K_\alpha$ radiation (wavelength 1.5406 Å). They were collected in the 2θ range of 20–80°, with a step size of 0.02° and a counting time of 0.5 s per step. In order to collect information preferentially from the disk surface, the grazing incidence diffraction method was applied using a grazing angle ω of 0.5°. In this method, the stationary incident beam makes a very small angle with the sample surface (typically 0.3–3°), which increases the path length of the X-ray beam through the coating. This helps to increase the diffracted intensity while at the same time reducing the diffracted intensity from the substrate, so the conventional phase identification analysis can be run. Fourier transform infrared (FTIR) spectra were collected with a Thermo Nicolet Nexus spectrometer (Thermo Scientific, USA) equipped with a Goldengate attenuated total reflectance (ATR) device. The contact angles were measured to estimate the wettability of the samples. The experiments were performed by the sessile drop method at 25 °C on a CAM 200 KSV contact angle goniometer. Pictures of the drops were taken every 1 s. The software delivered by the instrument manufacturer calculated the contact angles on the basis of a numerical solution of the full Young–Laplace equation.

Atomic force microscopy (AFM) measurements were performed using a Dimension Icon microscope from Bruker operating in non-contact mode. The probes were model TESP-SS, with a resonance frequency of around 300 kHz, a spring constant about 40 N $m^{-1}$ and a sharp spike tip at the end with a 2 nm nominal radius. The root mean square (RMS) roughness was measured in a $2 \times 2$ $\mu m^2$ area.

### 2.3. *In vitro osteoblast* cell cultures

Before in vitro assays of osteoblast cells, all samples were sterilized by dried heat at 150 °C for 12 h. Due to the presence of a $TiO_2$ phase on the surface of the samples when exposed to air, we intentionally avoided the use of ultraviolet light throughout the whole analysis of the samples to avoid any photoactive response of the layers [28]. The human osteoblast-like (HOS) cell line, obtained through the European Collection of Cell Cultures denoted HOS (ECACC, No. 87070202), was used. The cells were cultured in a complete medium consisting of Dulbecco's modified Eagle's medium (Sigma Chemical Co., St. Louis, USA) supplemented with 2 mM L-glutamine (Gibco, Invitrogen Corporation, USA), 100 U $ml^{-1}$ penicillin (Life Technologies Ltd., UK), 100 g $ml^{-1}$ streptomycin (Life Technologies Ltd.) and 10% fetal bovine serum (Gibco, Invitrogen Corporation, USA) at 37 °C in a humidified atmosphere of 95% air and 5% $CO_2$. Osteoblast-like cells were routinely subcultured by trypsinization. Then HOS cells were seeded onto the different samples previously placed into 24-well culture plates



Please cite this article in press as: Izquierdo-Barba I et al. Nanocolumnar coatings with selective behavior towards osteoblast and *Staphylococcus aureus* proliferation. Acta Biomater (2015), http://dx.doi.org/10.1016/j.actbio.2014.12.023

at a seeding density of $2.5 \times 10^5$ cells per ml in the complete medium under a $CO_2$ (5%) atmosphere at 37 °C for different time periods for each in vitro assay.

*2.3.1. Cell adhesion assay*

For cell attachment experiments, samples were incubated under standard culture conditions for 90 min. The samples were then washed three times in phosphate-buffered saline (PBS; Sigma–Aldrich Life Science), after which the cells attached to the different surfaces were unattached by trypsin treatment for 10 min. The cells were centrifuged, resuspended in PBS and counted in a Neubauer chamber. Data are expressed as means ± standard deviations of three experiments. Tissue culture plastic was used as a control.

*2.3.2. Cell-spreading assays*

The attached cells were rinsed three times in PBS and fixed with 2.5% glutaraldehyde (50 wt.%; Sigma–Aldrich, USA) in PBS for 45 min. Sample dehydration was performed by slow water replacement, using a series of ethanol solutions (30, 50, 70 and 90%) for 30 min, with a final dehydration in absolute ethanol for 60 min, allowing samples to dry at room temperature and in a vacuum. Thereafter, the samples were mounted on stubs and gold coated in a vacuum using a sputter coater (Balzers SCD 004, Liechtenstein) and visualized by scanning electron microscopy (SEM) using a field emission JEOL JSM-6335F microscope (Tokyo, Japan) at an acceleration voltage of 10 kV.

*2.3.3. Cell mitochondrial activity*

Cell proliferation was determined in terms of cell mitochondrial activity. For this purpose, HOS cells were seeded onto the material surface in 24-well plates at a density of $10^5$ cells per ml in the complete medium and incubated under standard conditions. Cell proliferation determinations were performed using the MTT (3-[4,5-dimethylthiazol-2-yl]-2,5-diphenyltetrazolium bromide; Sigma–Aldrich, USA) assay at different time periods after seeding. Tissue culture plastic was used as control.

*2.3.4. Statistics of the biocompatibility assays*

Data are expressed as means ± standard deviations of three experiments. Statistical analysis was performed using the Statistical Package for the Social Sciences (SPSS), version 11.5 software. Statistical comparisons were made by analysis of variance. Scheffé's test was used for post hoc evaluations of differences among groups. In all statistical evaluations, $p < 0.05$ was considered to be statistically significant.

*2.4. Bacteria in vitro tests*

*2.4.1. Bacterial adhesion test*

Prior to the bacterial adhesion tests, Ti6Al4V and Nano-Ti6Al4V samples were sterilized by dried heat at 150 °C for 12 h. The bacterial adhesion studies were performed on different Ti6Al4V surfaces using the *S. aureus* 15981 laboratory strain and six clinical strains identified as P1, P2, P4, P18, P61T3 and P95. The clinical strains were isolated, using a sonication procedure, from patients who had had an orthopedic implant-related infection. For the adhesion experiments, bacteria were inoculated in tryptic soy broth (TSB; BioMerieux, Marcy L'Etoile, France) and incubated overnight at 37 °C with 5% $CO_2$. After culture, bacteria were centrifuged for 10 min at 3500g at 22 °C. The supernatant was then discarded and the pellet was washed three times with sterile PBS. The bacteria were then suspended and diluted in PBS to obtain a concentration of $10^8$ colony-forming units per ml; the bacterial concentration was determined by spectrophotometry using a visible spectrophotometer (Genesys 20, Thermo Scientific). Different specimens of Ti6Al4V were inoculated with the bacterial solutions for 90 min to allow adhesion in a static model. The samples were then washed three times with PBS to remove any unattached bacteria. Finally, they were stained for 15 min with a Live/Dead® Bacterial Viability Kit (BacklightTM). Staining was performed with a mixture of dyes: SYTO 9 (live bacteria/green) and propidium iodide (dead bacteria/red). SYTO 9 fluorescence was excited at 480/500 nm, with the emitted fluorescence measured at 500 nm, and propidium iodide fluorescence was excited at 490/635 nm, with the emitted fluorescence measured at 618 nm [28]. Eight photographs (40× magnification) were taken of each sample using an ultraviolet microscope. The surface area covered with adhered bacteria was calculated using ImageJ software (National Institute of Health, Bethesda, MD). The experiments were performed in triplicate for each strain.

*2.4.2. Confocal microscopy*

Confocal microscopy studies were carried out with a Biorad MC1025 confocal laser scanning microscope. The different specimens were stained with BacklightTM dye, as previously described.

*2.4.3. Biofilm formation test*

Both surfaces were suspended in a bacterial solution of *S. aureus* strain ($10^8$ bacteria $ml^{-1}$) and incubated for 24 h in a 66% TSB + 0.2% glucose medium to promote robust biofilm formation (20 g $l^{-1}$ of Difco Bacto tryptic soy broth, Becton Dickinson, Sparks, MD). After 24 h, both surfaces were washed three times with sterile PBS, stained with 3 µl of Syto-9/propidium iodide mixture, incubated for 15 min and washed with PBS.

To specifically determine the biofilm formation, we used calcofluor, a fluorescent dye that has been used to stain the extracellular matrix of biofilms. In this case, 1 ml of calcofluor solution (5 mg $ml^{-1}$) was inoculated after the addition of the Syto-9/propidium iodide mixture and was incubated for 15 min at room temperature. Biofilm formation was examined using a LEICA SP2 Confocal Laser Scanning Microscope. Confocal 3-D image reconstruction was carried out from 45 Z stacks in an Olympus FV1200 confocal microscope.

*2.4.4. Statistics for bacterial studies*

The results obtained were presented, comparing the mean percentage of covered biomaterial surface for the untreated and sputtered specimens, respectively, using EPI-INFO software version 3.5.1 (CDC, Atlanta, GA). To carry out the statistical study, nonparametric tests were performed.

## 3. Results and discussion

The SEM micrographs in Fig. 1 show the different surface features between Ti6Al4V (Fig. 1a) and Nano-Ti6Al4V (Fig. 1b). After MS-GLAD, the Nano-Ti6Al4V substrate appears fully coated, with patterns on the nanoscale. The nanotopography of the analyzed coatings consists of almost vertically aligned nanocolumns with lengths between 250 and 350 nm and diameters between 40 and 60 nm, separated (from center to center) by 100–200 nm (Fig. 1c and d). In this way, the coating fully covers the Ti6Al4V material, with numerous nanofeatures per unit area. It has been described that this kind of dense, highly packed nanotopography, together with the separation between nanofeatures, can lead to a significant decrease in wettability due to a "lotus leaf effect" on the material surface [29–31]. In order to estimate the wettability of the samples, contact angles measurements were carried out. Despite the fact that the measured contact angle does not classify Nano-Ti6Al4V as superhydrophobic, the wettability of the Ti6Al4V sub-

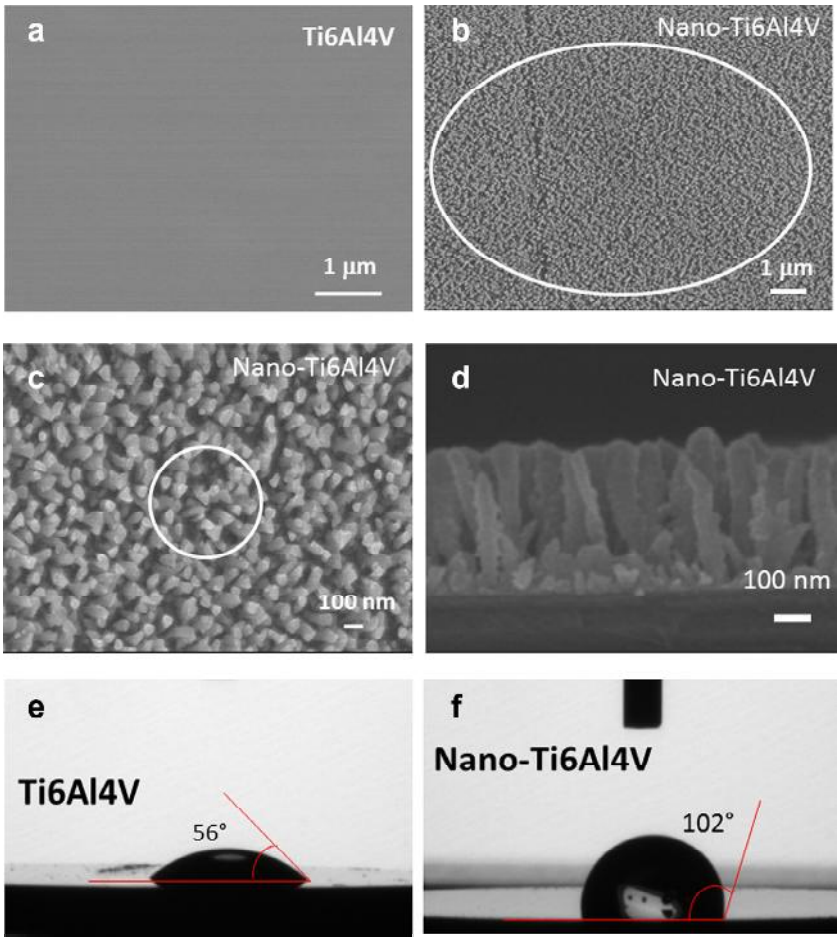


**Fig. 1.** SEM micrographs of (a) Ti6Al4V substrate; (b) Nano-Ti6Al4V sample; the selected area gives an estimation of the osteoblast size; (c) Nano-Ti6Al4V; selected area gives an estimation of the *S. aureus* size; (d) SEM image of a Nano-Ti6Al4V cross-section showing the nanocolumns. Evaluation of surface wettability; (e) micrograph of a water drop on a Ti6Al4V substrate sample. (f) Micrograph of a water drop on a Nano-Ti6Al4V sample.

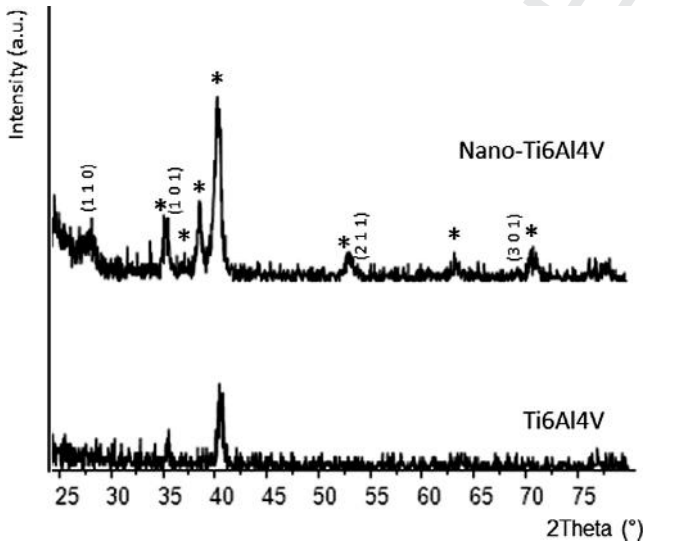


**Fig. 2.** XRD patterns of Nano-Ti6Al4V (top) and Ti6Al4V (bottom) samples collected with grazing incidence angle ($\Omega = 0.5°$). Miller indexes are indicated for the $TiO_2$ rutile phase. Asterisks indicate the diffraction maxima corresponding to α-Ti.

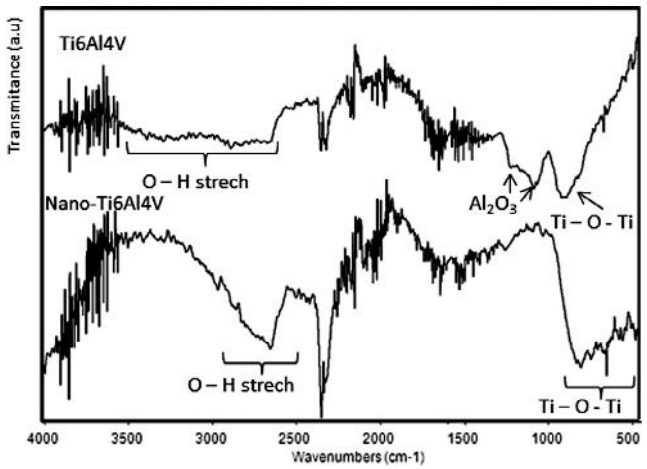


**Fig. 3.** FTIR spectra of Nano-Ti6Al4V (bottom) and Ti6Al4V (top) samples collected by ATR.

strate dramatically decreases after being coated with the Ti nanocolumns (Fig. 1e and f). The contact angle for the initial Ti6Al4V substrate is 56°, whilst that of Nano-Ti6Al4V is 102°.

Fig. 2 shows the grazing incidence XRD patterns for Ti6Al4V and Nano-Ti6Al4V. The maxima for Ti6Al4V alloy can be assigned to the hexagonal α-Ti phase (the major phase in Ti6Al4V alloys), with space group *P63/mmc*. However, the pattern corresponding to Nano-Ti6Al4V also shows diffraction maxima that can be assigned

Please cite this article in press as: Izquierdo-Barba I et al. Nanocolumnar coatings with selective behavior towards osteoblast and *Staphylococcus aureus* proliferation. Acta Biomater (2015), http://dx.doi.org/10.1016/j.actbio.2014.12.023

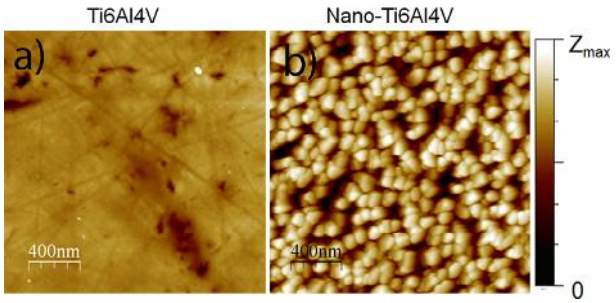


**Fig. 4.** AFM images of Ti6Al4V (a) and Nano-Ti6Al4V (b), the color scale for the height being $Z_{max}$ = 46 nm and $Z_{max}$ = 380 nm for Ti6Al4V and Nano-Ti6Al4V, respectively.

to $TiO_2$ rutile phase, with space group *P42/mm*. These results indicate the presence of crystalline $TiO_2$ rutile on the Nano-Ti6Al4V samples. This oxide layer is formed when exposing the material to the atmosphere, which induces the oxidation of the first atomic monolayers, as evidenced by the $TiO_2$ maxima found in the XRD pattern.

ATR-FTIR spectroscopy results are shown in Fig. 3. FTIR spectra obtained by means of the ATR method mainly collect information from the sample surfaces. The spectra collected for Ti6Al4V show absorption bands between 2550 and 3550 $cm^{-1}$. This wide interval of vibrations corresponds to the stretching vibration of O–H bonds in different situations at the alloy surface, i.e. isolated Ti–OH groups, undergoing intermolecular forces, polymeric units, adsorbed water, etc. [32]. The bands at 1200 and 1083 $cm^{-1}$ correspond to the phonon mode vibration of $Al_2O_3$ [33] (commonly present in Ti6Al4V alloys). Finally, the band at 916 $cm^{-1}$ can be assigned to the Ti–O–Ti vibrational mode, thus indicating the presence of a thin titanium oxide layer on the substrate, commonly present in these alloys as consequence of dry passivation.

The FTIR spectrum for Nano-Ti6Al4V shows similar absorption bands. However, there are significant differences in the width of the frequency interval. For instance, the band assigned to the O–H stretching vibration is centered in a lower frequency interval between 2900 and 2600 $cm^{-1}$. This indicates that hydroxyls groups with the lower O–H energy bond predominate at the surface of Nano-Ti6Al4V, which is indicative of electron charge transference due to hydrogen bonding between neighboring hydroxyl groups. The vibrational modes of Ti–O–Ti appear in a wide interval of frequencies from 950 to 500 $cm^{-1}$, which is indicative of different states of the $TiO_2$ layer being present on the Nano-Ti6Al4V surface. The phonon mode vibration of $Al_2O_3$ does not appear in the FTIR spectra for Nano-Ti6Al4V. The FTIR spectra of Nano-Ti6Al4V collected by ATR indicate a more ordered arrangement of Ti–OH groups, where OH groups would be close enough to form hydrogen bonds, as deduced from the prevalence of the stretching O–H signals at lower frequencies. In contrast, FTIR spectra obtained for

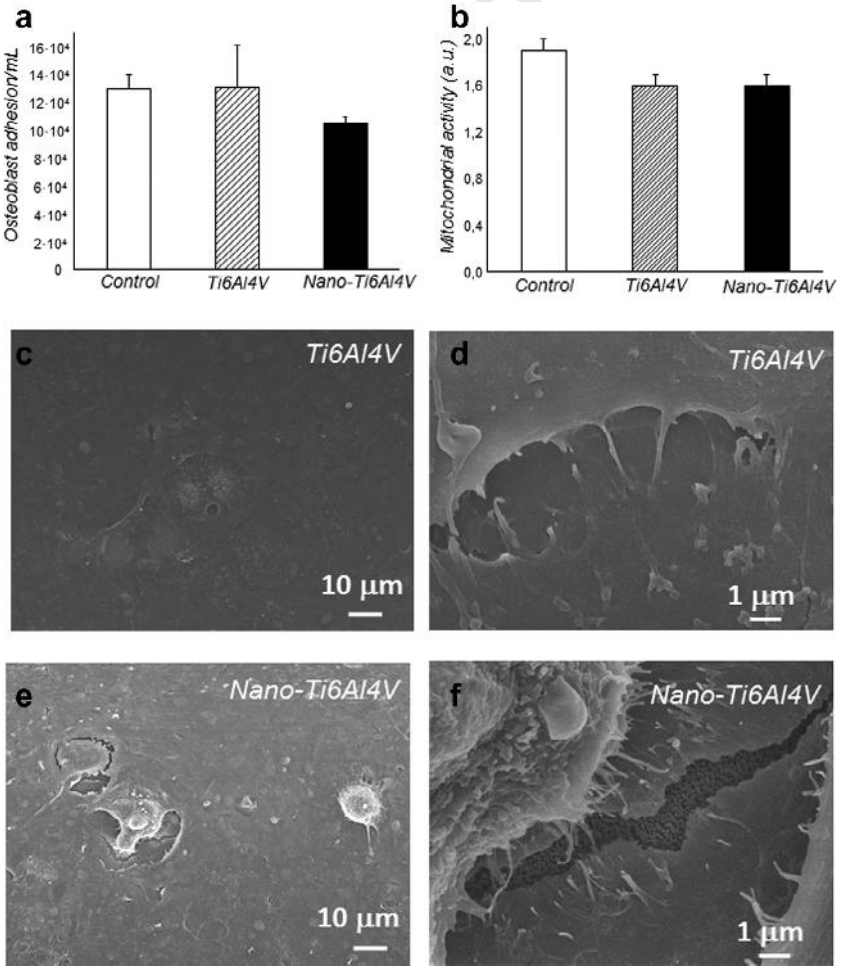


**Fig. 5.** Osteoblast adhesion after 90 min on a Ti6Al4V substrate and a Nano-Ti6Al4V sample (a). Mitochondrial activity (MTT test) after 3 days of osteoblast culture on Ti6Al4V and Nano-Ti6Al4V (b). SEM micrographs obtained after 24 h of culture with osteoblast cells on a Ti6Al4V substrate (c and d) and a Nano-Ti6Al4V sample (e and f). Non-statistically significant ($p > 0.05$) differences were observed in both the osteoblast adhesion (a) and MTT tests (b).

Please cite this article in press as: Izquierdo-Barba I et al. Nanocolumnar coatings with selective behavior towards osteoblast and *Staphylococcus aureus* proliferation. Acta Biomater (2015), http://dx.doi.org/10.1016/j.actbio.2014.12.023

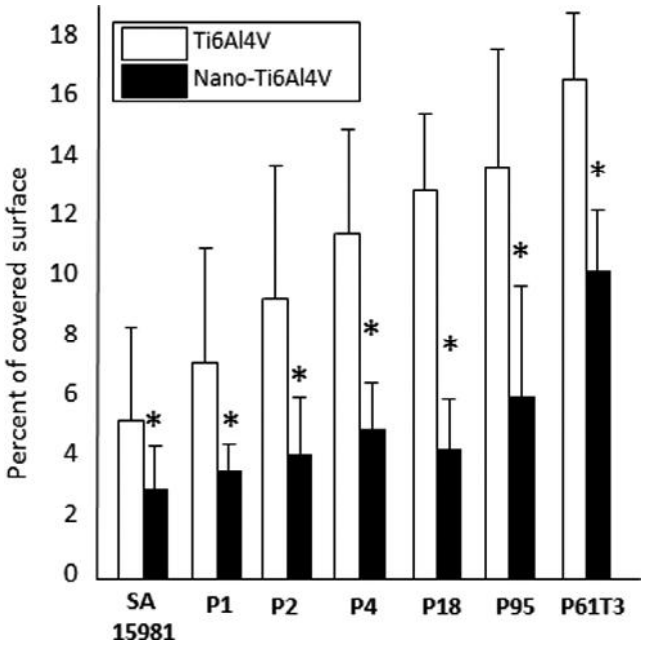


**Fig. 6.** Bacterial adhesion tests carried out by inoculation of *S. aureus* 15981collection strain and several clinical strains onto Ti6Al4V and Nano-Ti6Al4V surfaces. *Significant differences, $p < 0.001$, Kruskal–Wallis test.

Ti6Al4V indicate a more disordered arrangement of the Ti–OH groups. Both XRD and FTIR results indicate the formation of crystalline rutile over the nanocolumn topography, whereas the $TiO_2$ layer formed over polished substrates seems to be a non-ordered phase.

AFM measurements were performed to characterize the nanotopography of the Ti6Al4V substrates (Fig. 4a) and the Nano-Ti6Al4V samples (Fig. 4b). The Ti6Al4V substrates exhibit several scratches, due to the mechanical polishing, and the RMS roughness of the whole $2 \times 2$ $\mu m^2$ area is about 3 nm. After the growth of the coating by magnetron sputtering, the surface of Nano-Ti6Al4V is homogeneously coated with Ti nanocolumns, as can be clearly seen in Fig. 4b. The measured RMS roughness is 57 nm in this case, although this value must be understood as an underestimation, since the AFM tip could not penetrate down to the very bottom of some inter-columnar spaces due to their high aspect ratio.

Once both Ti6Al4V and Nano-Ti6Al4V surfaces had been characterized, we proceeded to evaluate the in vitro biocompatibility by culturing the HOS cell line on them. The initial (90 min) osteoblast adhesion (Fig. 5a) does not show significant differences between the medical grade Ti6Al4V substrate, the Nano-Ti6Al4V sample and the control. Also, the mitochondrial activities of HOS are almost identical for Ti6Al4V and Nano-Ti6Al4V, and do not show any significant difference after 3 days of culture (Fig. 5b). The observation of the surfaces by SEM after 1 day of culture (Fig. 5c–f) confirmed that Nano-Ti6Al4V behaves as well as medical grade Ti6Al4V with respect to human osteoblasts. The surfaces in both cases appear fully covered by cells, exhibiting good adhesion, proliferation and degree of extension. Higher magnification images (Fig. 5d and f) show the anchoring elements spread by the cells. In the case of Nano-Ti6Al4V, Fig. 5f shows the details of a broken cell, which allows the Ti nanocolumns remaining below the osteoblast layer to be observed.

Once the biocompatibility of the Nano-Ti6Al4V had been assessed, we studied the behavior of the Ti nanocolumns when exposed to *S. aureus*: not only to the collection strain 15981, but also to the six clinical strains, P1, P2, P4, P18, P61T3 and P95, isolated from different patients [34]. The antibacterial effect of the Nano-Ti6Al4V surfaces was observed by means of bacterial adhesion experiments and compared with those on medical grade Ti6Al4V substrates. Nano-Ti6Al4V exhibits a notable decrease in *S. aureus* adhesion for both the collection and clinical strains, although an interspecies variability exists (Fig. 6). The adhesion of strain 15981 *S. aureus* observed on the Nano-Ti6Al4V surface shows a significant decrease ($p < 0.001$, Kruskal–Wallis test) of around 70% with respect to the untreated Ti6Al4V surfaces. Furthermore, for the six clinical strains, which exhibit different degrees of initial bacterial adhesion, a significant decrease ($p < 0.001$, Kruskal–Wallis test) in the percentage of covered surface is also observed, reducing by ~68, 71, 69, 66 and 44% for the P1, P2, P4, P18, P95 and P61T3 strains, respectively.

Concerning biofilm formation, our initial observations by SEM after 24 h of culture showed that *S. aureus* 15981 developed an extracellular matrix that coated the Ti6Al4V substrates (Fig. 7). In contrast, the surface of Nano-Ti6Al4V appeared free of extracellular matrix. This observation impelled us to carry out appropriated studies for biofilm formation assessment. With this purpose in mind, we performed confocal microscopy to characterize the sequential biofilm formation after different times period using Syto-9/propidium iodide dyes, which label live and dead bacteria in green and red, respectively (Fig. 8a). In agreement with the previous SEM results, the presence of a few scattered bacteria on the Nano-Ti6Al4V surface is noted, as well as the absence of biofilm after 24 h of incubation. The thickness of the biological material attached to both surfaces was determined by analyzing eight different areas of each piece by confocal microscopy. The measured thickness was $21.8 \pm 3.3$ μm for the Ti6Al4V substrate ($n = 8$; $p < 0.001$, Kruskal–Wallis test), whilst the statistical software gave $4.8 \pm 7.8$ μm for Nano-Ti6AlV, an invalid value that means that there is only scattered bacteria on the surface, i.e. no biofilm is formed in this case. These measurements, together with the confocal microscopy images, clearly show a compact biofilm layer

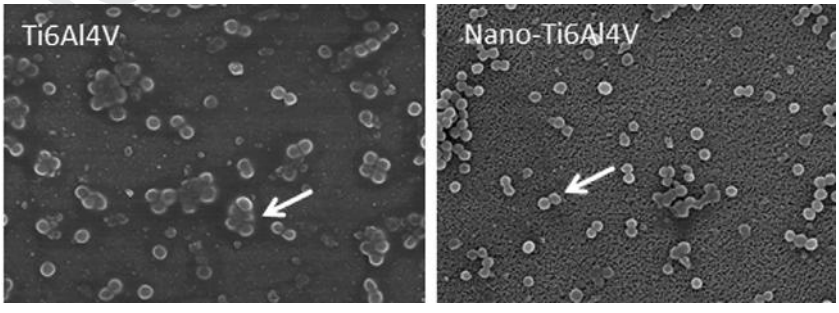


**Fig. 7.** SEM micrographs of Ti6Al4V (left) and Nano-Ti6Al4V (right) samples after 24 h of culture with *S. aureus*. The micrographs show the formation of a biofilm on the Ti6Al4V, whereas nanoroughness is still visible on the Nano-Ti6Al4V. In the Ti6Al4V, bacteria covered by extracellular matrix (arrow), which is an essential part of a biofilm, are observed. In the Nano-Ti6Al4V sample, only bacterial cells without the production of extracellular matrix are observed (arrow).

Please cite this article in press as: Izquierdo-Barba I et al. Nanocolumnar coatings with selective behavior towards osteoblast and *Staphylococcus aureus* proliferation. Acta Biomater (2015), http://dx.doi.org/10.1016/j.actbio.2014.12.023

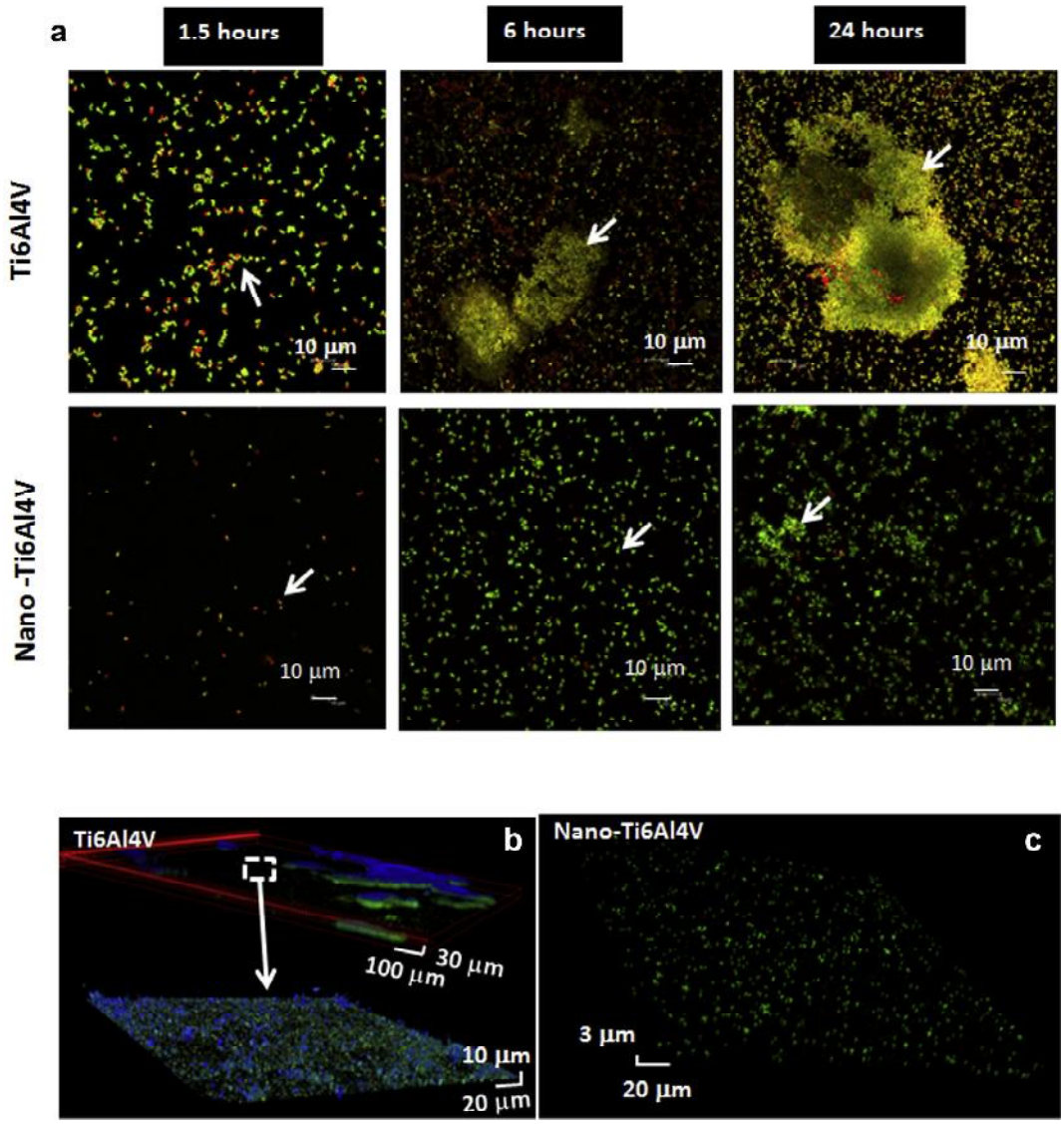


**Fig. 8.** (a) Images collected by confocal fluorescence microscopy after 1.5, 6 and 24 h of culture with *S. aureus* on Ti6Al4V and Nano-Ti6Al4V surfaces. Ti6Al4V shows initial bacterial adherence (1.5 h, arrow) and the subsequent development of a biofilm (6 and 24 h, arrows). Biofilms can be seen as bacterial conglomerates embedded in the extracellular matrix (arrows). No biofilms are observed in the modified material Nano-Ti6Al4V, and only cells and small conglomerates can be seen (arrows); (b) confocal 3-D reconstruction of the Ti6Al4V surface after 24 h of culture. Both extracellular matrix and bacteria are observed. (c) Confocal 3-D reconstruction of Nano-Ti6Al4V surface after 24 h of culture. Only live individual bacterial cells can be detected, with no biofilm formation.

covering the entire non-modified surface of Ti6Al4V and scattered bacterial adhesion on the nanostructured Nano-Ti6Al4V surface.

To further analyze these findings, we decided to carry out additional confocal microscopy experiments employing both Syto-9/propidium iodide (to distinguish live and dead bacteria) and calcofluor fluorescent stains (to stain the extracellular matrix of biofilms). Fig. 8b shows the confocal 3-D images corresponding to biofilm formation after 24 h of incubation. Non-coated Ti6Al4V substrates clearly show biofilm formation by the blue staining of typical extracellular matrix covering the bacterial colonies. In contrast, blue staining is absent in Nano-Ti6Al4V, as can be observed in Fig. 8c.

The selective behavior acquired by the Nano-Ti6AlV biomedical alloy can be explained taking into account the morphology of the sample surface at the nanoscale, the cell characteristics and surface chemistry modifications. In general, the cellular response to topographical features on metallic materials is cell-type dependent [35]. Typical osteoblast sizes range between 10 and 50 µm, and the osteoblasts possess a flexible cell membrane that allows them to adapt to different nanotopographies. Moreover, a necessary condition for them to adhere to a surface is the adsorption of integrins, a mechanism that is diminished on materials with chemical hydrophobic surfaces. In the light of our results, and the excellent adhesion of osteoblasts onto both Ti6Al4V and Nano-Ti6Al4V, it seems that osteoblasts exhibit little sensitivity to the topological features of the studied surfaces. Although a clear conclusion on this issue is far beyond the scope of this paper, our results suggest that the morphologically induced hydrophobicity of the Nano-Ti6Al4V does not prevent integrins from being absorbed by the surface, allowing the formation of complexes known as focal contacts, which attach the osteoblasts to the surface [18,36,37]. After this adhesion, the osteoblasts develop filopodia and lamellipodia to probe the environment, anchoring and moving, as well as allowing the biointegration of the material. In this regard, some studies in the literature have demonstrated that a corrugated topography with surface nanofeatures (grooves ridges, pits, etc.) separated by distances of the order of micrometers can influence cell adhesion [38–41]. In our case, the high density of nanocolumns and the very short



Please cite this article in press as: Izquierdo-Barba I et al. Nanocolumnar coatings with selective behavior towards osteoblast and *Staphylococcus aureus* proliferation. Acta Biomater (2015), http://dx.doi.org/10.1016/j.actbio.2014.12.023

distance between them (about 100 nm) seems to be undetectable by such large cells as osteoblasts, and these nanostructured surfaces would appear to be almost smooth with regard to their anchoring elements, as can be observed in Fig. 1b. In contrast, staphylococci are about 1 μm in diameter, and their cell walls are much more rigid than eukaryotic cells. In general, bacteria have a characteristic shape, and are not very deformable. Due to their smaller size, bacteria are sensitive to the nanotopography and to the nanocolumns. In fact, as was previously pointed out by Mitik-Dineva et al. [42], our study shows that bacteria are susceptible to nanoscale surface roughness. Specifically, the high density of nanocolumns seems to force *S. aureus* to attach to Nano-Ti6Al4V samples through a limited number of anchoring points at the top of the nanocolumns (about 20–30 nanocolumns, as can be estimated from Fig. 1c), thus reducing the area available for bacterial attachment. Together with the lotus leaf effect exhibited by these nanosurfaces, the adhesion of *S. aureus* onto Nano-Ti6Al4V is strongly impeded. Although the chemical properties of biofilms may vary depending upon the microbial species, the adhesion of bacteria (both specific and unspecific) is a mandatory stage in biofilm formation. In this sense, the physico-chemical interaction between surface and bacteria plays a fundamental role in the adhesion stage [43]. Our findings indicate that the nanocolumns prepared by MS-GLAD exert a very important influence on biofilm inhibition by acting on the unspecific stage of bacterial growth.

## 4. Conclusion

Titanium nanocolumnar coatings provide new perspectives for manufacturing Ti6Al4V-based implants for bone tissue repair, as they demonstrate the possibility of manufacturing drug-free surfaces that simultaneously exhibit opposing responses to osteoblasts and *S. aureus*.

## Acknowledgements

Q7 Q8 This study was supported by research Grants from the Ministerio de Ciencia e Innovación (MICINN) through the projects MAT2012-35556 and CSO2010-11384-E (Agening Network of Excellence), The Spanish MINECO (Projects CONSOLIDER CSD2 008-00023, MAT2011-29194-C02-01, MAT2013-40852-R and MAT2013-43299-R) and the Junta de Andalucía (projects P12-FQM-2265 and P10-FQM-6900).

## Appendix A. Figures with essential color discrimination

Certain figures in this article, particularly Figs. 1, 4 and 8 are difficult to interpret in black and white. The full color images can be found in the on-line version, at http://dx.doi.org/10.1016/j.actbio.2014.12.023.

## References

[1] Arcos D, Boccaccini AR, Bohner M, Díez-Pérez A, Epple M, Gomez-Barrena E, et al. The relevance of biomaterials to the prevention and treatment of osteoporosis. Acta Biomater 2014;10:1793–805.
[2] Campoccia D, Montanaro L, Ariola CR. The significance of infection related to orthopedic devices and issues of antibiotic resistance. Biomaterials 2006;27:2331–9.
[3] Gioe TJ, Killeen KK, Grimm K, Mehle S, Scheltema K. Why are total knee replacements revised? Analysis of early revision in a community knee implant registry. Clin Orthop Relat Res 2004;428:100–6.
[4] Fitzgeral RH. Prevention and diagnosis. Orthop Clin N Am 1992;23:259–64.
[5] Urban JA, Garvin KL. Prosthetic joint infection. Curr Treat Options Infect Dis 2003;413:261–8.
[6] Foster TJ. The *Staphylococcus aureus* "superbug". J Clin Invest 2004;114:1693–6.
[7] Harris LG, Richards RG. *Staphylococcus aureus* adhesion to different treated titanium surfaces. J Mater Sci – Mater Med 2004;15:311–4.
[8] Götz F. Staphylococcus and biofilms. Mol Microbiol 2002;43:1367–78.
[9] Konig C, Schwank S, Blaser J. Factors compromising antibiotic activity against biofilms of *Staphylococcus epidermidis*. Eur J Clin Microbiol Infect Dis 2001;20:20–6.
[10] Stewart PS. Mechanisms of antibiotic resistance in bacterial biofilms. Int J Med Microbiol 2002;292:107–13.
[11] Campoccia D, Montanaro L, Arciola CR. A review of the biomaterials technologies for infection-resistant surfaces. Biomaterials 2013;34:8533–54.
[12] Puckett SD, Taylor E, Raimondo T, Webster TJ. The relationship between the nanostructure of titanium surfaces and bacterial attachment. Biomaterials 2010;31:706–13.
[13] Díaz C, Schilardi PL, Salvarezza RC, Fernández-Lorenzo M, Mele D. Nano/microscale order affects the early stages of biofilm formation on metal surfaces. Langmuir 2007;23:11206–10.
[14] Jahed Z, Lin P, Seo BB, Verma MS, Gu FX, Tsui TY, et al. Responses of *Staphylococcus aureus* bacterial cells to nanocrystalline nickel nanostructures. Biomaterials 2014;35:4249–54.
[15] Webster TJ, Ejiofor JU. Increased osteoblast adhesion on nanophase metals: Ti, Ti6Al4V, CoCrMo. Biomaterials 2004;25:4731–9.
[16] de Oliveira PT, Zalzal SF, Beloti MM, Rosa AL, Nanci A. Enhancement of in vitro osteogenesis on titanium by chemically produced nanotopography. J Biomed Mater Res 2007;80A:554–64.
[17] Webster TJ, Ergun C, Doremus RH, Siegel RW, Bizios R. Enhanced functions of osteoblasts on nanophase ceramics. Biomaterials 2000;21:1803–10.
[18] Anselme K, Davidson P, Popa AM, Giazzon M, Ploux L. The interaction of cells and bacteria with surfaces structures at the nanometre scale. Acta Biomater 2010;6:3824–46.
[19] Colon G, Ward BC, Webster TJ. Increased osteoblast and decreased *Staphylococcus epidermidis* functions on nanophase ZnO and $TiO_2$. J Biomed Mater Res A 2006;78:595–604.
[20] Ploux L, Anselme K, Dirani A, Ponche A, Soppera O, Roucoules V. Opposite responses of cells and bacteria to micro/nanopatterned surfaces prepared by pulsed plasma polymerization and UV-irradiation. Langmuir 2009;25:8161–9.
[21] Mei S, Wang H, Wang W, Tong L, Pan H, Ruan C, et al. Antibacterial effects and biocompatibility of titanium surfaces with graded silver incorporation in titania nanotubes. Biomaterials 2014;35:4255–65.
[22] Decuzzi P, Ferrari M. Modulating cellular adhesion through nanotopography. Biomaterials 2010;31:173–9.
[23] Sengstock C, Lopian M, Motemani Y, Borgmann A, Khare C, Buenconsejo PJS, et al. Structure-related antibacterial activity of a titanium nanostructured surface fabricated by glancing angle sputter deposition. Nanotechnology 2014;25:195101.
[24] Alvarez R, García-Martín JM, Macías-Montero M, González-García L, González JC, Rico V, et al. Growth regimes of porous gold thin films deposited by magnetron sputtering at oblique incidence: from compact to columnar microstructures. Nanotechnology 2013;24:045604.
[25] Sit JC, Vick D, Robbie K, Brett MJ. Thin film microstructure control using glancing angle deposition by sputtering. J Mater Res 1999;14:1197–9.
[26] Kelly PJ, Arnell RD. Magnetron sputtering: a review of recent developments and applications. Vacuum 2000;56:159–72.
[27] García-Martín JM, Alvarez R, Romero-Gómez P, Cebollada A, Palmero A. Tilt angle control of nanocolumns grown by glancing angle sputtering at variable argon pressures. Appl Phys Lett 2010;97:173103.
[28] Terriza A, Díaz-Cuenca A, Yubero F, Barranco A, González-Elipe AR, González-Caballero JL, et al. Light induced hydrophilicity and osteoblast adhesion promotion on amorphous $TiO_2$. J Biomed Mater Res A 2013;101A:1026–35.
[29] Ivanova EP, Hasan J, Webb HK, Truong VK, Watson GS, Watson JA, et al. Natural bactericidal surfaces: mechanical rupture of *Pseudomonas aeruginosa* cells by cicada wings. Small 2012;8:2489–94.
[30] Guo Z, Liu W, Su BL. Superhydrophobic surfaces: from natural to biomimetic to functional. J Coll Interf Sci 2011;353:335–55.
[31] Singh DP, Singh JP. Enhanced evaporation of sessile water droplet on vertically standing Ag nanorods film. J Phys Chem C 2011;15:11914.
[32] Kumar DA, Xavier JA, Shya JM, Xavier FP. Synthesis and structural, optical and electrical properties of $TiO_2/SiO_2$ nanocomposites. J Mater Sci 2013;48:3700–7.
[33] Dillon AC, Ott AW, Way JD, George SM. Surface chemistry of $Al_2O_3$ deposition using $Al(CH_3)_3$ and $H_2O$ in a binary reaction sequence. Surf Sci 1995;322:23042.
[34] Arenas MA, Perez-Jorge C, Conde A, Matykina E, Hernandez-Lopez JM, Perez-Tanoira de Damborenea JJ, et al. Doped TiO2 anodic layers of enhanced antibacterial properties. Colloids Surf B Biointerfaces 2013;105:106–12.
[35] Ross AM, Jiang Z, Bastmeyer M, Lahann J. Physical aspects of cell culture substrates: topography, roughness, and elasticity. Small 2012;8:336–55.
[36] Anselme K. Osteoblast adhesion on biomaterials. Biomaterials 2000;21:667–81.
[37] Hunter A, Archer CW, Walker PS, Blunn GW. Attachment and proliferation of osteoblasts and fibroblasts on biomaterials for orthopaedic use. Biomaterials 1995;16:287–95.
[38] Links J, Boyan BD, Blanchard CR, Lohmann CH, Liu Y, Cochran DL, et al. Response of MG63 osteoblast-like cells to titanium and titanium alloy is dependent on surface roughness and composition. Biomaterials 1998;19:2219–32.
[39] Fuita S, Ohshia M, Iwaa H. Time-lapse observation of cell alignment on nanogrooved patterns. J R Soc Interface 2009;6:S269–77.

[40] Texeira AI, Abrams GA, Bertics PJ, Murphy CJ, Nealey PF. Epithelial contact guidance on well-defined micro- and nanostructured substrates. J Cell Sci 2003;116:1881–92.
[41] Loesberg WA, Riet J, van Delft FCMJM, Schön P, Figdor CG, Speller S. The threshold at which substrate nanogroove dimensions may influence fibroblast alignment and adhesion. Biomaterials 2007;22:3944–51.
[42] Mitik-Dineva N, Wang J, Mocanasu RC, Stoddart PR, Crawford RJ, Ivanova EP. Impact of nano-topography on bacterial attachment. Biotechnol J 2008;3:536–44.
[43] Ploux L, Ponche A, Anselme K. Bacteria/material interfaces: role of the material and cell wall properties. J Adhesion Sci Technol 2010;24:2165–201.



Please cite this article in press as: Izquierdo-Barba I et al. Nanocolumnar coatings with selective behavior towards osteoblast and *Staphylococcus aureus* proliferation. Acta Biomater (2015), http://dx.doi.org/10.1016/j.actbio.2014.12.023